Carbon 140 (2018) 441–448

Contents lists available at ScienceDirect

Carbon

journal homepage: www.elsevier.com/locate/carbon

Efficient removal of bisphenol-A by ultra-high surface area porous activated carbon derived from asphalt

Hassan Javed [a, b], Duy X. Luong [a, b, c], Chang-Gu Lee [a, d], Danning Zhang [a, e], James M. Tour [a, b], Pedro J.J. Alvarez [a, e, *]

[a] NSF Nanosystems Engineering Research Center for Nanotechnology Enabled Water Treatment (NEWT), USA
[b] Dept. of Chemistry, Rice University, Houston, TX 77005, USA
[c] Applied Physics Program, Rice University, 6100 Main Street, Houston, TX, 77005, USA
[d] Dept. of Environmental and Safety Engineering, Ajou University, Suwon, South Korea
[e] Dept. of Civil and Environmental Engineering, Rice University, Houston, TX 77005, USA

ARTICLE INFO

Article history:
Received 16 July 2018
Received in revised form
10 August 2018
Accepted 19 August 2018
Available online 28 August 2018

ABSTRACT

An ultra-high surface area porous activated carbon derived from low cost asphalt (AS) was synthesized and investigated for removal of bisphenol A (BPA), a common endocrine disrupting chemical (EDC) in wastewater and natural waters. Adsorption isotherms, kinetics and thermodynamics of BPA adsorption were determined and benchmarked against commercially purchased Darco G-60 activated carbon (AC). The surface area of AS was 3851 m^2/g, which is 4.7-fold larger than that of AC (i.e., 813 m^2/g). This correlates well with the 4-fold higher maximum BPA adsorption capacity on AS (1113 ± 52 mg/g), and is consistent with the similar surface functionality of AS and AC (determined by Fourier-transform infrared spectroscopy). The maximum BPA adsorption capacity of AS is highest among reported carbon materials. BPA adsorption kinetics by both materials was limited by slow intraparticle diffusion into the small mesopores and micropores, which resulted in slightly slower adsorption rate for AS that had a greater proportion of micropores than AC. Thermodynamic analysis corroborated that BPA adsorption was favorable and occurred predominantly through π-π interaction as indicated by Raman spectroscopy. Overall, AS is a highly efficient adsorbent for removal of EDCs for water purification and could be considered for drinking water treatment and wastewater polishing.

1. Introduction

Endocrine disrupting chemicals (EDCs) have gained considerable attention as contaminants of emerging concern. EDCs can affect the normal function of hormones leading to various health implications such as interference with the reproductive systems of aquatic animals [1,2]. Bisphenol A (BPA) is a commonly encountered EDC that has been widely used in the production of polycarbonates, epoxy resins and other plastics [3–6]. BPA can adversely affect aquatic life due to its endocrine disruption activity and oxidative and mutagenic potential [3,7]. BPA has been detected in varying concentrations in hazardous waste landfill leachate (17.2 mg/L) [8], stream water (12 μg/L) [9], and drinking water (0.317 μg/L) [10]. The reported concentrations at which BPA induces endocrine effects vary widely, with reported values ranging from 1 to 1000 μg/L [11]. Removal of BPA during water and wastewater treatment is, therefore, important to ensure human health and protect aquatic life.

Activated carbon is widely used in water treatment to remove taste and odor compounds, synthetic organic contaminants and some heavy metals [12–15]. The octanol/water partition coefficient (K_{ow}) of an organic contaminant is a good indicator of how effectively it can be removed by activated carbon. Generally, contaminants with log K_{ow} >2 are effectively removed by adsorption onto activated carbon [16]. BPA with its log K_{ow} value of 3.32 is, therefore, well-suited for removal by activated carbon-based materials [17].

A number of characteristics including pore structure, ash content, functional groups and surface area can contribute to the adsorption efficiency of activated carbons [18]. Pore structure and surface area are very important parameters as high surface area and

* Corresponding author. NSF Nanosystems Engineering Research Center for Nanotechnology Enabled Water Treatment (NEWT), USA.
E-mail address: alvarez@rice.edu (P.J.J. Alvarez).

https://doi.org/10.1016/j.carbon.2018.08.038
0008-6223/

easily accessible pores can significantly increase adsorption capacity. Ultra-high surface area asphalt-derived activated carbon (AS) has been previously synthesized, with surface areas achievable up to 4200 m^2/g [19]. This material was considered for competitive adsorption of CO_2 in carbon capture efforts. AS, with its ultra-high surface area, offers high adsorption capacity for water purification. In this paper, we investigate its application for BPA adsorption in an aqueous environment. We report adsorption isotherms, kinetics and thermodynamics of BPA adsorption and benchmark the results against commercially purchased activated carbon.

2. Materials and methods

2.1. Materials

Untreated Gilsonite was provided by Prince Energy. Potassium hydroxide (KOH) (≥85% purity), acetone (ACS reagent, ≥99.5% purity), acetonitrile (HPLC Plus, ≥99.9% purity) and bisphenol A (≥99% purity) were purchased from Sigma Aldrich. Darco G-60 activated carbon (AC) was purchased from Fisher Chemical. Polytetrafluoroethylene (PTFE) syringe filters with 0.2 μm pore size were purchased from VWR International. Deionized (DI) water (>18.2 MΩ) used for washings and solution preparations was prepared by Millipore (Milli-Q Academic) water purification system.

2.2. Synthesis of AS

AS was synthesized using the KOH activation method [19], which yields higher surface area activated carbon than steam activation and has also been previously used to prepare ultra-high surface area 3D graphene-based bulk materials [20–22]. Untreated Gilsonite was chosen as the carbon source as it gives a much higher surface area activated carbon compared to other carbon sources that we have previously tested (Table S1). Briefly, Gilsonite (1.50 g) was heated on a ceramic boat under Ar in a tube furnace at 400 °C for 3 h to remove the oils and obtain a stable ensuing pore structure; this material was then allowed to cool to room temperature to form 0.50 g of pretreated Gilsonite. 0.25 g of the pretreated Gilsonite was then ground well with 1 g of KOH in a mortar. The mixture was transferred to a quartz boat and heated in the tube furnace at 900 °C for 20 min under Ar flow. This generates CO and CO_2, which opens the pore structure. After the mixture had cooled to room temperature, it was washed with acetone and water until the filtrate had attained pH 7. This yielded AS (0.10–0.15 g) which was then dried in an oven at 100 °C until constant weight before further use.

2.3. BPA adsorption experiments

Adsorption isotherms were obtained by adding 10 mg of adsorbent (100 mg/L) to a beaker containing 100 mL of BPA solution at different concentrations (50–200 mg/L for AS, 10–100 mg/L for AC). A low adsorbent concentration (100 mg/L) was needed to obtain data on residual (non-adsorbed) BPA for adsorption isotherms and thermodynamic analysis. The solutions were stirred continuously for 4 h to achieve adsorption equilibrium, after which 1 mL sample aliquot was withdrawn and filtered through 0.2 μm PTFE filter for analysis. For adsorption kinetics experiments, 10 mg of adsorbent (100 mg/L) were added to a beaker containing 100 mL of 50 mg/L BPA solution. The solutions were continuously stirred. 1 mL sample aliquots were withdrawn at 5, 10, 15, 20, 25, 30, 60, 120, 180, 240 min intervals and filtered for further analysis. Temperature controlled experiments to investigate thermodynamics of adsorption on AS were carried out by adding 10 mg of AS to a beaker containing 100 mL of 150 mg/L BPA solution. The beaker was sealed with parafilm and the solutions were stirred continuously. The temperature of the solutions was controlled using a thermocouple probe equipped hot plate. The experiments were conducted at 23, 45 and 65 °C. Samples for analysis were taken after 4 h equilibration time.

2.4. Adsorption isotherm, kinetics and thermodynamics models

Two common adsorption isotherm models were considered to fit the data. The Langmuir isotherm [23,24] is given by Equation (1):

$$q = Q_{max} * \frac{K_L * C_e}{1 + K_L * C_e} \tag{1}$$

Where q is the amount of solute adsorbed onto adsorbent (mg/g), C_e is the equilibrium concentration of solute remaining in solution (mg/L), K_L is the Langmuir constant (L/mg) and Q_{max} is the maximum adsorption capacity (mg/g).

The Freundlich isotherm [23,25] is given by Equation (2):

$$q = K_f C_e^{1/n} \tag{2}$$

Where K_f and 1/n are system-specific constants. K_f indicates adsorption capacity $((mg/g)\cdot(L/mg)^{1/n})$ and 1/n indicates intensity of adsorption where a higher 1/n value indicates more favorable adsorption.

Two adsorption kinetics models were also considered. The pseudo 1st order model [26] is given by Equation (3):

$$\frac{dq_t}{dt} = k_1(q_e - q_t) \tag{3}$$

Which is integrated as (Equation (4)):

$$\ln(q_e - q_t) = lnq_e - k_1 t \tag{4}$$

Where q_e is the amount of solute adsorbed at equilibrium (mg/g), q_t is the amount of solute adsorbed at time t (mg/g), and k_1 is the pseudo first order rate constant (1/min).

The pseudo 2nd order kinetic model [26] is given by Equation (5):

$$\frac{dq_t}{dt} = k_2(q_e - q_t)^2 \tag{5}$$

Which is integrated as (Equation 6)

$$\frac{t}{q_t} = \frac{1}{k_2 q_e^2} + \frac{t}{q_e} \tag{6}$$

Where k_2 is the pseudo second order rate constant (g/(mg·min)).

An intraparticle diffusion model [27] was also used to assess whether the rate of intraparticle diffusion was limiting overall adsorption kinetics (Equation (7)).

$$q_t = k_p t^{\frac{1}{2}} \tag{7}$$

Where k_p is the intraparticle diffusion rate constant $(mg/(g\cdot h^{1/2}))$.

Thermodynamic parameters of adsorption were calculated by determining the solute (linear) distribution coefficient (K_d) at different equilibrium temperatures [28] as follows:

$$K_d = \frac{C_{Ae}}{C_e} \tag{8}$$

$$\Delta G^{\circ} = -RTlnK_d \tag{9}$$

$$lnK_d = \frac{\Delta S^{\circ}}{R} - \frac{\Delta H^{\circ}}{RT} \tag{10}$$

Where C_{Ae} is amount of solute adsorbed at equilibrium (mg/L) and C_e is the equilibrium concentration of solute in solution (mg/L). R and T are gas constant (8.314 J/(mol·K)) and temperature (K) respectively. ΔG°, ΔH° and ΔS° are standard free energy (J/mol), standard enthalpy (J/mol) and standard entropy (J/mol), respectively.

2.5. Characterization methods

Scanning electron microscope (SEM) images were obtained on Quanta 400 ESEM equipped with field emission gun (FEI, now Thermo Fisher Scientific). High resolution transmission electron microscope (HRTEM) images were obtained in a JEOL 2100 field emission gun TEM (JEOL Ltd.). X-ray diffraction (XRD) was measured using Rigaku D/Max Ultima II Powder X-ray diffractometer (Rigaku Corporation) equipped with a Cu Kα radiation source (λ = 1.5418 A). Raman spectrum were measured on a Renishaw Raman microscope (Renishaw) using a 514 nm Ar ion laser with a power of 5 mW. Surface area (Brunauer-Emmett-Teller (BET)) and pore size distributions (Horvath-Kawazo (HK) and Barrett-Joyner-Halenda (BJH)) were measured using Autosorb-3B (Quantachrome Instruments). Fourier-transform infrared spectroscopy (FTIR) was performed on Nicolet FTIR Infrared Microscope (Thermo Fisher Scientific). X-ray photoelectron spectroscopy of the samples was performed on PHI Quantera SXM Scanning Photoelectron Spectrometer Microprobe (Physical Electronics, Inc.).

2.6. Analytical methods

BPA was analyzed using a high performance liquid chromatography (LC20AT, Shimadzu, Japan) equipped with a C-18 column (Atlantis dC18 Column, 100 Å, 3 μm, 3.9 mm × 150 mm) and an UV−Vis photodiode array detector (SPD-M20A, Shimadzu, Japan). 60% acetonitrile and 40% water were used as the mobile phase. The flow rate and injection volume were 1.0 mL/min and 40 μL, respectively. The zeta potential of AS and AC were determined with a Zen 3600 Zetasizer Nano (Malvern Instruments, UK) by phase analysis light scattering.

3. Results and discussion

3.1. Adsorbents characterization

SEM and HRTEM images of AC and AS are given in Fig. 1a−d. Both carbon materials had different morphology with internal macroporous channels visible for AC (Fig. 1a). HRTEM images show that both materials were primarily amorphous. However, small crystalline regions with lattice spacing of 3.4 Å were observed at the edges of AS (Fig. 1d). The presence of small crystalline regions in both carbons was also later confirmed by XRD and Raman spectroscopy. AS and AC exhibited different N_2 adsorption-desorption profiles (Fig. 2). AS followed type Ib adsorption isotherm while AC followed type IIb adsorption isotherm of the IUPAC 1985 classification of physisorption isotherms [29]. Type Ib indicates monolayer adsorption or a relatively small amount of multilayer adsorption, and is typical for microporous materials exhibiting cooperative filling of wider micropores at a range of higher P/P_0 than Type Ia materials [29,30]. Type IIb isotherm is associated with multilayer adsorption and indicates adsorption into larger mesopores. AC adsorption-desorption isotherm also exhibited a type H_4 hysteresis loop which is characteristic of materials with slit-shaped pores [30,31]. The surface area of AS synthesized for this study was 4.7 times higher than that of AC (Table 1). The total pore volume of AS was 2.9 times higher than AC. AS exhibited a smaller average pore diameter of 2.5 nm compared to average pore diameter of 4 nm for AC. The pore volume distributions were also different for both materials. AS had a higher proportion of micropores than AC (Table 1). Microspores constituted 70% of the total pore volume for AS, whereas, they constituted only 45% of the total pore volume for AC. The different average pore diameter and pore volume distributions may partially explain the observed difference in N_2 adsorption-desorption profiles. AC with its higher mesopore to micropore volume ratio would provide more unrestricted access that facilitates multilayer adsorption, while AS with its higher micropore population provides more confined cavities favoring monolayer adsorption. The central linear part in the AC N_2 adsorption-desorption isotherm corresponds to monolayer adsorption which may likely correspond to monolayer adsorption in its micropores (Fig. 2b).

XRD analysis of AC and AS indicates that both materials are primarily amorphous, and no sharp peaks are observed in the XRD pattern (Fig. 3a). The 002 and 010 peaks are clearly visible for AC while a small 010 peak can be identified for AS. The 002 and 010 peaks correspond to crystalline regions of diffraction from layering of graphitic carbons and formation of small 2D lattices, respectively [19]. XRD analysis reveals that both materials exhibit small regions of crystallinity arising from sp2-hybridized graphitic system, with AC displaying more graphitic character than AS. The surface functionality of both carbon materials was probed using FTIR (Fig. 3b). Both materials give identical FTIR spectra, indicating the presence of identical surface functional groups. The 880 cm^{-1} peak corresponds to C−H out-of-plane bending in benzene derivatives while the 1070 cm^{-1} corresponds to C−O stretches of primary alcohol groups. The 1170 cm^{-1} and 1270 cm^{-1} peaks may correspond to C−O stretches of aliphatic ether and alkyl aryl ethers, respectively. The 1400 cm^{-1} and 1680 cm^{-1} absorbances correspond to aromatic and alkene C=C stretches, respectively. The 2850 cm^{-1} and 2920 cm^{-1} peaks both correspond to C−H bending. A weak broad band from 3100 cm^{-1} to 3400 cm^{-1} is also visible in FTIR spectrum of both materials corresponding to O−H stretches. Both FTIR spectrums had a peak at 2370 cm^{-1} which corresponds to the C=O stretches of ambient CO_2 molecules. The presence of similar functional groups on both materials was corroborated by XPS analysis (Figure S1, Table S2). Both materials were negatively charged under the tested conditions (Table S3).

3.2. BPA adsorption isotherms

Langmuir and Freundlich adsorption isotherms were fitted to BPA adsorption on AS and AC (Fig. 4 and Table 2). The maximum adsorption capacity of AS was 1113 ± 52 mg/g, which was 4 times higher than the maximum adsorption capacity of 271 ± 14 mg/g for AC, as determined from Langmuir isotherm. Similarly, K_f determined from Freundlich isotherm was also 4 times higher for AS compared to AC, indicating 4 times higher adsorption capacity. The adsorption data relates well with the surface areas of both materials as AS had 4.7 times higher surface area than AC. This proportionality was expected as surface functionality of both was determined to be quite similar based on FTIR and XPS analysis. This is also corroborated by similar 1/n values for both AS and AC which indicate that BPA adsorption was equally favorable on both materials. Overall, AS provides the largest surface area and highest adsorption capacities reported to date for BPA adsorption by carbon-based materials (Table 3).

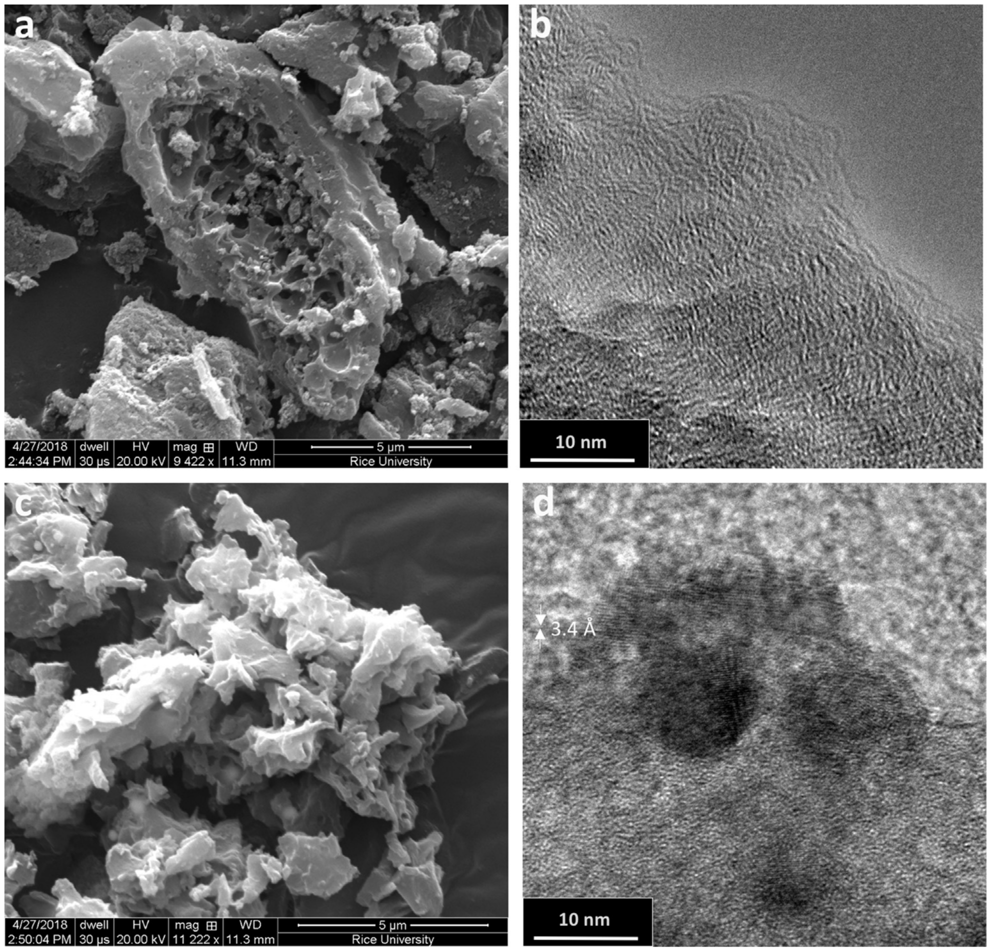

Fig. 1. (a) and (c) are SEM images of AC and AS, respectively. Internal macroporous channels are visible for AC. (c) And (d) are HRTEM images of AC and AS, respectively. Both carbons are largely amorphous; however, small crystalline regions are observed at the edges of AS with average lattice spacing of 3.4 Å.

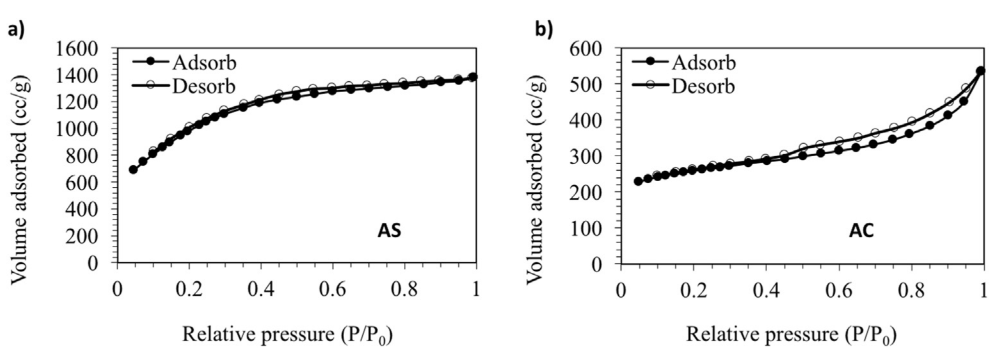

Fig. 2. N_2 adsorption-desorption isotherms for a) AS and b) AC. AS followed type Ib (monolayer) adsorption isotherm while AC followed type IIb (multilayer) adsorption isotherm.

Table 1
Surface area and pore volume characterizations of AS and AC.

	BET surface area	Total pore volume	Average pore diameter D_p	Mesopore volume	Micropore volume
	m^2/g	cc/g	nm	cc/g	cc/g
AS	3851 ± 494	2.366 ± 0.324	2.46 ± 0.02	0.616 ± 0.112	1.538 ± 0.192
AC	813 ± 5	0.822 ± 0.009	4.04 ± 0.07	0.484 ± 0.023	0.390 ± 0.004

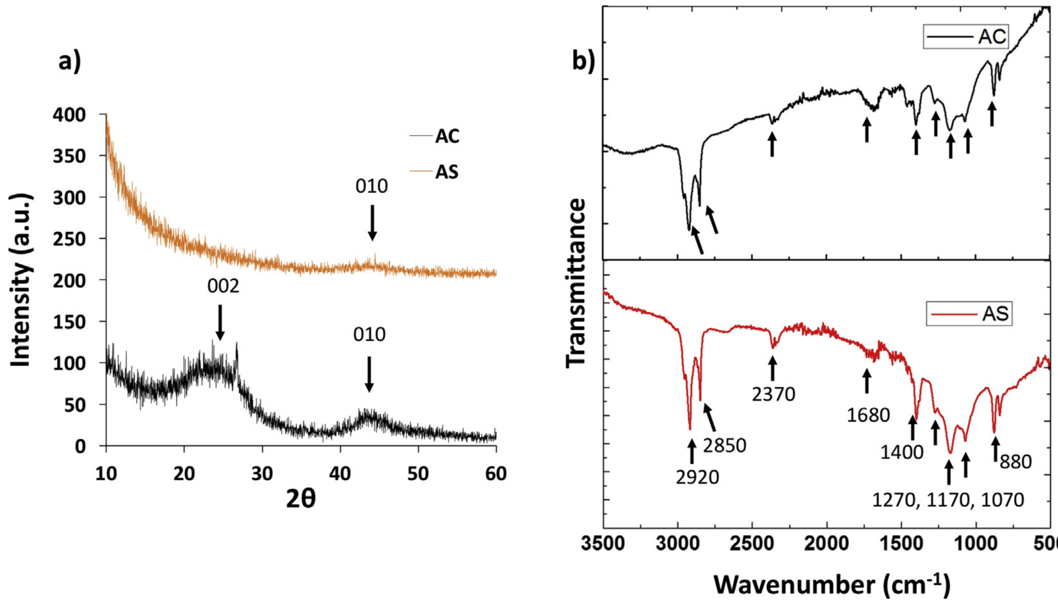

Fig. 3. a) XRD of AS and AC. 010 and 002 peaks are clearly visible for AC while a weak 010 peak is observed for AS. These peaks indicate presence of small crystallinity in both materials. b) FTIR spectra of AC and AS. The FTIR spectra of both materials show a high degree of similarity with identical peak positions, indicating presence of similar surface functional groups. (A colour version of this figure can be viewed online.)

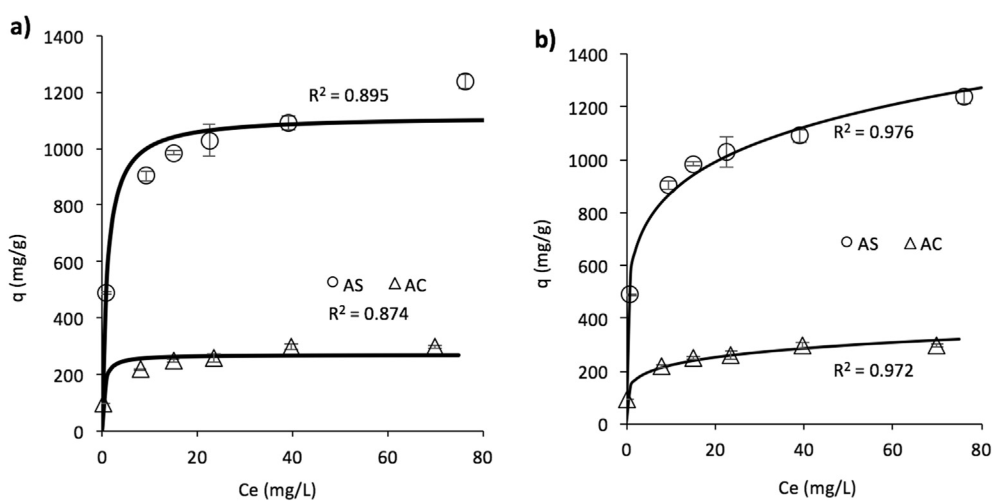

Fig. 4. a) Langmuir and b) Freundlich adsorption isotherms for BPA adsorption on AS and AC. AS exhibits a four-fold higher adsorption capacity than AC in both isotherms.

Table 2
Adsorption parameters calculated from Langmuir and Freundlich isotherms.

	Langmuir			Freundlich		
	Q_m	K_L	R^2	K_f	1/n	R^2
	(mg/g)	(L/mg)		$(mg/g)\cdot(L/mg)^{1/n}$		
AS	1113 ± 52	0.92 ± 0.34	0.895	577 ± 33	0.18 ± 0.02	0.976
AC	271 ± 14	2.36 ± 1.24	0.874	145 ± 10	0.18 ± 0.02	0.972

3.3. Kinetics of BPA adsorption

Pseudo 1st order and pseudo 2nd order models were fit to the kinetic data of BPA adsorption on AS and AC (Fig. 5 and Table 4). The kinetics of BPA adsorption on both materials was slightly better described by pseudo 2nd order model (AS, R^2: 0.999; AC, R^2: 0.998) than pseudo 1st order model (AS, R^2: 0.991; AC, R^2: 0.982). Both materials exhibited fast kinetics for BPA adsorption. The pseudo 2nd order rate constant for AC (0.00263 ± 0.00024 g/(mg·min)) was higher than the rate constant for AS (0.00166 ± 0.00001 g/(mg·min)), indicating slightly faster adsorption kinetics for AC. To further gain insights into the kinetics of BPA adsorption on the two carbonaceous materials, an intraparticle diffusion model was fit to the kinetics data (Fig. 6). The graph of q_t vs $t^{1/2}$ shows multi-linearity, indicating multi-stage adsorption of BPA on both AC and AS. The multi-stage adsorption behavior of contaminants on activated carbons has been previously reported [32,33]. A number of parameters can limit the adsorption kinetics of adsorbate on adsorbent including diffusion coefficient of the adsorbate in the bulk phase, concentration of adsorbate and degree of mixing, among others. However, under well-mixed and high-adsorbate concentration conditions used in our experiments, intraparticle diffusion is often the rate limiting step [32,34,35]. In Fig. 6, three stages with different adsorption rates are observable for AS and AC.

Table 3
Comparison of BPA adsorption on different types of carbon materials.

Material	Surface Area (m^2/g)	Langmuir		Freundlich		Reference
		Q_m (mg/g)	K_L (L/mg)	K_f (mg/g)·$(L/mg)^{1/n}$	1/n	
AS	**3851**	**1113.2**	**0.9**	**576.9**	**0.181**	**This Study**
AC	**813**	**270.7**	**2.4**	**145.2**	**0.182**	
AC-Olive Mill waste	1641	589.0	0.1	NA	NA	[5]
AC-Commercial	1225	164.4	0.1	NA	NA	[5]
AC from Potato Peel	905	445.9	0.1	64.9	0.366	[36]
AC-Commercial	1326	319.4	0.3	82.8	0.473	[43]
AC-Commercial	824	NA	NA	123.0	0.213	[44]
AC-Commercial	957	NA	NA	54.7	0.330	
Nitrogen-modified mesoporous carbon	580	240.4	0.3	88.5	0.269	[45]
Goethite/AC composite	522	NA	NA	187.2	2.089	[46]
Mesoporous carbon	920	296.0	0.1	55.1	0.450	[47]
AC-Commercial	1060	328.3	5.0	253.8	0.140	[4]
AC-Commercial	1158	303.0	0.1	NA	NA	[38]

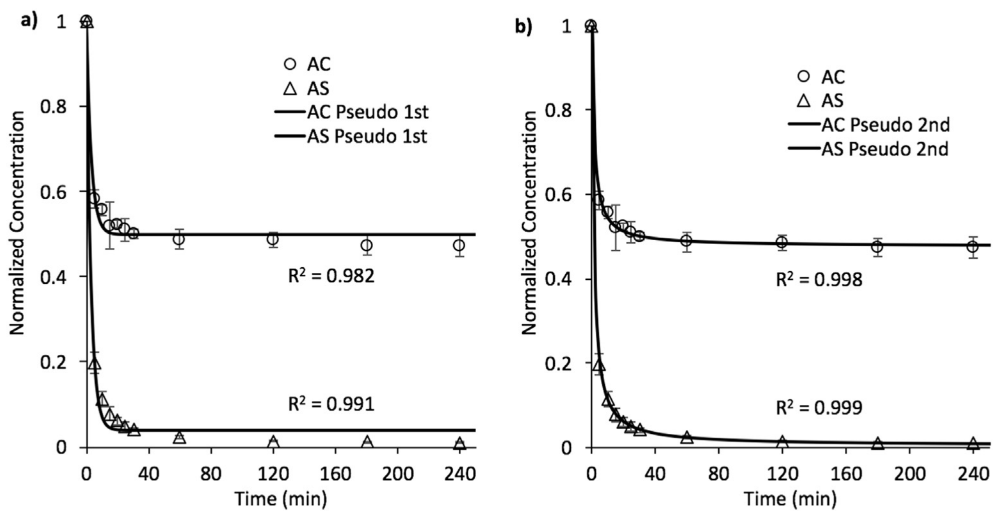

Fig. 5. Kinetics of BPA adsorption on AS and AC fitted by a) Pseudo 1st order model and b) Pseudo 2nd order model. BPA was adsorbed onto 10 mg of adsorbent from 100 mL of 50 mg/L BPA stock solution. The 2nd order model provided a slightly better data fit. AS and AC exhibited very similar adsorption kinetics with AC giving slightly faster adsorption rate. The high adsorption capacity of AS is observable, as within 4 h, AS removed 99% BPA compared to 53% for AC.

Table 4
Kinetic parameters calculated from pseudo 1st order and pseudo 2nd order kinetics models.

	Pseudo 1st order			Pseudo 2nd order		
	k_1 (1/min)	q_e (mg/g)	R^2	k_2 (g/(mg·min))	q_e (mg/g)	R^2
AS	0.336 ± 0.030	481.1 ± 4.6	0.991	0.00166 ± 0.00001	498.1 ± 0.2	0.999
AC	0.316 ± 0.042	250.6 ± 3.8	0.982	0.00263 ± 0.00024	261.4 ± 1.8	0.998

The first stage represents fast external surface adsorption or boundary layer diffusion. The second and third stage represent slower adsorption rates limited by intraparticle diffusion. The second stage corresponds to the diffusion of BPA into the macropores and wider mesopores of the AS and AC. The third portion represents the slowest adsorption rate, limited by intraparticle diffusion of BPA into the small mesopores and micropores of AS and AC [33]. The intraparticle diffusion model demonstrates that for both AS and AC, BPA diffusion into the small mesopores and micropores was the rate limiting step. This provides some insight into why the adsorption rate for AC was slightly faster than AS. AS with higher proportion micropores (70% of the total pore volume) compared to AC (45% of the total pore volume) is likely to be more affected by the rate limited adsorption of BPA into the small micropores than AC, thereby exhibiting a slightly lower net adsorption rate.

3.4. Thermodynamics and mechanism of adsorption

The thermodynamic parameters for BPA adsorption on AS were computed from the plot of K_d and 1/T (Figure S2) and are summarized in Table 5. Negative values were obtained for ΔG° indicating spontaneous and favorable adsorption over the tested temperatures. BPA adsorption onto AS was an exothermic reaction as indicated by the negative ΔH°. Furthermore, decrease in ΔG° was observed with increase in temperature. This is expected due to the exothermic nature of BPA adsorption on AS which makes higher temperatures less favorable for adsorption. ΔS° was negative due to the restriction in movement of BPA molecules after adsorption onto AS surface [36]. Moreover, ΔG° was within the range of 0 to −20 kJ/mol which indicated that BPA adsorption on AS occurred primarily through a physical adsorption process rather than a chemical

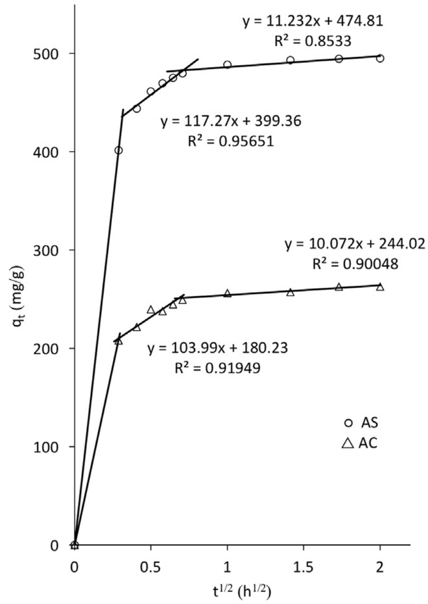

Fig. 6. Intraparticle diffusion model fitting of the BPA adsorption kinetics for AS and AC.

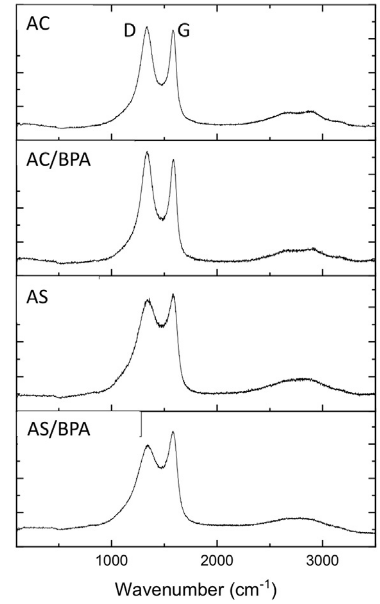

Fig. 7. Raman spectrum of AC and AS with and without BPA adsorption. Small shifts in D and G bands were observed for both AS and AC after BPA adsorption, indicative of π-π interactions between BPA and sp2-hybridized network of both materials.

Table 5
Thermodynamic parameters for BPA adsorption on AS.

Temp (°C)	ΔG° (KJ/mol)	ΔH° (KJ/mol)	ΔS° (J/mol)
23	−2.51 ± 0.05	−9.8 ± 0.2	−24.7 ± 0.5
45	−1.95 ± 0.04		
65	−1.48 ± 0.04		

Table 6
Shifts in D and G peaks in the Raman spectrum of AS and AC after BPA adsorption.

	Peak positions (cm^{-1})	
	D	G
AS	1360	1583
AS/BPA	1366	1584
AC	1337	1578
AC/BPA	1339	1580

process [37]. This aligns well with the widely accepted mechanism of BPA adsorption on carbon-based materials which is expected to proceed through π-π interaction between the aromatic rings of activated carbon and BPA [38]. To further probe the mechanism of adsorption of BPA on AS, Raman spectroscopy was used. Several researchers have used Raman spectroscopy to investigate adsorption of target molecules onto graphene based materials through π-π interaction [39–41]. The adsorbed molecules can act as electron donors/acceptors through π-π interaction and modify the electronic structure of graphene, leading to shifts in G and D band positions [39]. As AS and AC both had aromatization and exhibited sp2-hybridized graphitic character, Raman spectroscopy was used to investigate the mechanism of adsorption. The Raman spectrum of both materials gave distinct G and D bands (Fig. 7). The G band corresponds to the E_{2g} in-plane vibration mode of sp2-hybridized carbon while the D band arises from disorder in the sp2-hybridized system [42]. A subtle shift to higher frequency was observed for both G and D bands in case of AS and AC after BPA adsorption which indicates that adsorption of BPA on AC and AS proceeded primarily through π-π interaction (Table 6). For AS, the D band and G band shifted from 1360 cm^{-1} and 1583 cm^{-1} to 1366 cm^{-1} and 1584 cm^{-1} respectively after BPA adsorption. While for AC, the D band and G band shifted from 1337 cm^{-1} and 1578 cm^{-1} to 1339 cm^{-1} and 1580 cm^{-1}, respectively, after BPA adsorption.

4. Conclusion

AS was highly efficient for adsorption of BPA and should also be tested for removal of other organic contaminants of emerging concern from water. Its high surface area correlated well with its four-fold higher BPA adsorption capacity than that of commercial AC. In fact, with 1113 ± 52 mg/g, AS has the highest BPA adsorption capacity of all reported carbon materials. The adsorption of BPA on AS was thermodynamically favorable and proceeded through π-π interaction. For both AC and AS, diffusion of BPA into the small mesopores and micropores was determined as the rate limiting step. Further improvements such as enhancing the selectivity of AS towards BPA by modifying surface functionality and controlling pore structure may result in more efficient utilization of adsorption capacity and enhance the feasibility of AS for targeted removal of micropollutants from wastewater effluents.

Acknowledgements

This research is supported by the NSF ERC on Nanotechnology-Enabled Water Treatment (EEC-1449500). We thank Xifan Zhang for his help with the TEM analysis.

Appendix A. Supplementary data

Supplementary data related to this article can be found at https://doi.org/10.1016/j.carbon.2018.08.038.

References

[1] C.R. Tyler, S. Jobling, J.P. Sumpter, Endocrine disruption in wildlife: a critical

review of the evidence, Crit. Rev. Toxicol. 28 (1998) 319–361, https://doi.org/10.1080/10408449891344236.
[2] S. Jobling, D. Casey, T. Rodgers-Gray, J. Oehlmann, U. Schulte-Oehlmann, S. Pawlowski, T. Baunbeck, A.P. Turner, C. Tyler, Comparative responses of molluscs and fish to environmental estrogens and an estrogenic effluent, Aquat. Toxicol. 65 (2003) 205–220, https://doi.org/10.1016/S0166-445X(03)00134-6.
[3] J. Michałowicz, Bisphenol A – sources, toxicity and biotransformation, Environ. Toxicol. Pharmacol. 37 (2014) 738–758, https://doi.org/10.1016/J.ETAP.2014.02.003.
[4] W.-T. Tsai, C.-W. Lai, T.-Y. Su, Adsorption of bisphenol-A from aqueous solution onto minerals and carbon adsorbents, J. Hazard Mater. 134 (2006) 169–175, https://doi.org/10.1016/J.JHAZMAT.2005.10.055.
[5] M.I. Bautista-Toledo, J. Rivera-Utrilla, R. Ocampo-Pérez, F. Carrasco-Marín, M. Sánchez-Polo, Cooperative adsorption of bisphenol-A and chromium(III) ions from water on activated carbons prepared from olive-mill waste, Carbon N. Y. 73 (2014) 338–350, https://doi.org/10.1016/J.CARBON.2014.02.073.
[6] O.S. Alimi, J. Farner Budarz, L.M. Hernandez, N. Tufenkji, Microplastics and nanoplastics in aquatic environments: aggregation, deposition, and enhanced contaminant transport, Environ. Sci. Technol. 52 (2018) 1704–1724, https://doi.org/10.1021/acs.est.7b05559.
[7] M.Y. Chen, M. Ike, M. Fujita, Acute toxicity, mutagenicity, and estrogenicity of bisphenol-A and other bisphenols, Environ. Toxicol. 17 (2002) 80–86, https://doi.org/10.1002/tox.10035.
[8] T. Yamamoto, A. Yasuhara, H. Shiraishi, O. Nakasugi, Bisphenol A in hazardous waste landfill leachates, Chemosphere 42 (2001) 415–418, https://doi.org/10.1016/S0045-6535(00)00079-5.
[9] V.A. Santhi, N. Sakai, E.D. Ahmad, A.M. Mustafa, Occurrence of bisphenol A in surface water, drinking water and plasma from Malaysia with exposure assessment from consumption of drinking water, Sci. Total Environ. 427–428 (2012) 332–338, https://doi.org/10.1016/J.SCITOTENV.2012.04.041.
[10] S.M. Arnold, K.E. Clark, C.A. Staples, G.M. Klecka, S.S. Dimond, N. Caspers, S.G. Hentges, Relevance of drinking water as a source of human exposure to bisphenol A, J. Expo. Sci. Environ. Epidemiol. 23 (2013) 137–144, https://doi.org/10.1038/jes.2012.66.
[11] U.S. Environmental Protection Agency, Bisphenol-A Action Plan, 2010.
[12] C.J. Corwin, R.S. Summers, Controlling trace organic contaminants with GAC adsorption, J. Am. Water Works Assoc. 104 (2012) E36–E47, https://doi.org/10.5942/jawwa.2012.104.0004.
[13] I.N. Najm, V.L. Snoeyink, B.W. Lykins Jr., J.Q. Adams, Using powdered activated carbon: a critical review, J. Am. Water Works Assoc. 83 (1991) 65–76, https://doi.org/10.2307/41293123.
[14] T. Karanfil, J.E. Kilduff, Role of granular activated carbon surface chemistry on the adsorption of organic compounds. 1. Priority pollutants, Environ. Sci. Technol. 33 (1999) 3217–3224, https://doi.org/10.1021/ES981016G.
[15] C. van Lienden, L. Shan, S. Rao, E. Ranieri, T.M. Young, Metals removal from stormwater by commercial and non-commercial granular activated carbons, Water Environ. Res. 82 (2010) 351–356, https://doi.org/10.2175/106143009X12487095236874.
[16] C.H. Ward, H.F. Stroo, In Situ Remediation of Chlorinated Solvent Plumes, Springer, 2010.
[17] G.G. Ying, R.S. Kookana, P. Dillon, Sorption and degradation of selected five endocrine disrupting chemicals in aquifer material, Water Res. 37 (2003) 3785–3791, https://doi.org/10.1016/S0043-1354(03)00261-6.
[18] A. Dąbrowski, P. Podkościelny, Z. Hubicki, M. Barczak, Adsorption of phenolic compounds by activated carbon—a critical review, Chemosphere 58 (2005) 1049–1070, https://doi.org/10.1016/J.CHEMOSPHERE.2004.09.067.
[19] A.S. Jalilov, Y. Li, J. Tian, J.M. Tour, Ultra-high surface area activated porous asphalt for CO_2 capture through competitive adsorption at high pressures, Adv. Energy Mater. 7 (2017) 1600693, https://doi.org/10.1002/aenm.201600693.
[20] F.C. Wu, R.L. Tseng, C.C. Hu, Comparisons of pore properties and adsorption performance of KOH-activated and steam-activated carbons, Microporous Mesoporous Mater. 80 (2005) 95–106, https://doi.org/10.1016/J.MICROMESO.2004.12.005.
[21] L. Zhang, F. Zhang, X. Yang, G. Long, Y. Wu, T. Zhang, K. Leng, Y. Huang, Y. Ma, A. Yu, Y. Chen, Porous 3D graphene-based bulk materials with exceptional high surface area and excellent conductivity for supercapacitors, Sci. Rep. 3 (2013) 1408, https://doi.org/10.1038/srep01408.
[22] Y. Lu, G. Long, L. Zhang, T. Zhang, M. Zhang, F. Zhang, Y. Yang, Y. Ma, Y. Chen, What are the practical limits for the specific surface area and capacitance of bulk sp2 carbon materials? Sci. China Chem. 59 (2016) 225–230, https://doi.org/10.1007/s11426-015-5474-y.
[23] K.Y. Foo, B.H. Hameed, Insights into the modeling of adsorption isotherm systems, Chem. Eng. J. 156 (2010) 2–10, https://doi.org/10.1016/J.CEJ.2009.09.013.
[24] I. Langmuir, The constitution and fundamental properties of solids and liquids. Part I. Solids, J. Am. Chem. Soc. 38 (1916) 2221–2295, https://doi.org/10.1021/ja02268a002.
[25] H.M.F. Freundlich, Over the adsorption in solution, J. Phys. Chem. 57 (1906) 385–471.
[26] Y.S. Ho, Review of second-order models for adsorption systems, J. Hazard Mater. 136 (2006) 681–689, https://doi.org/10.1016/J.JHAZMAT.2005.12.043.
[27] W.J. Weber, J.C. Morris, Advances in water pollution research: removal of biologically resistant pollutant from waste water by adsorption, in: Proc. Int. Conf. Water Pollut. Symp., Pergamon Press, Oxford, UK, 1962, pp. 231–266.
[28] I.A.W. Tan, A.L. Ahmad, B.H. Hameed, Adsorption of basic dye on high-surface-area activated carbon prepared from coconut husk: equilibrium, kinetic and thermodynamic studies, J. Hazard Mater. 154 (2008) 337–346, https://doi.org/10.1016/J.JHAZMAT.2007.10.031.
[29] F. Rouquerol, J. Rouquerol, K.S.W. Sing, Adsorption by Powders and Porous Solids : Principles, Methodology, and Applications, Academic Press, 1999.
[30] M.C. Baquero, L. Giraldo, J.C. Moreno, F. Suárez-Garcia, A. Martinez-Alonso, J.M.D. Tascón, Activated carbons by pyrolysis of coffee bean husks in presence of phosphoric acid, J. Anal. Appl. Pyrolysis 70 (2003) 779–784, https://doi.org/10.1016/S0165-2370(02)00180-8.
[31] D. Prahas, Y. Kartika, N. Indraswati, S. Ismadji, Activated carbon from jackfruit peel waste by H_3PO_4 chemical activation: pore structure and surface chemistry characterization, Chem. Eng. J. 140 (2008) 32–42, https://doi.org/10.1016/J.CEJ.2007.08.032.
[32] E. Lorenc-Grabowska, G. Gryglewicz, Adsorption of lignite-derived humic acids on coal-based mesoporous activated carbons, J. Colloid Interface Sci. 284 (2005) 416–423, https://doi.org/10.1016/J.JCIS.2004.10.031.
[33] E. Lorenc-Grabowska, G. Gryglewicz, Adsorption characteristics of Congo Red on coal-based mesoporous activated carbon, Dyes Pigments 74 (2007) 34–40, https://doi.org/10.1016/J.DYEPIG.2006.01.027.
[34] A.S. Özcan, A. Özcan, Adsorption of acid dyes from aqueous solutions onto acid-activated bentonite, J. Colloid Interface Sci. 276 (2004) 39–46, https://doi.org/10.1016/J.JCIS.2004.03.043.
[35] A. Kumar, S. Kumar, S. Kumar, Adsorption of resorcinol and catechol on granular activated carbon: equilibrium and kinetics, Carbon N. Y. 41 (2003) 3015–3025, https://doi.org/10.1016/S0008-6223(03)00431-7.
[36] A.C. Arampatzidou, E.A. Deliyanni, Comparison of activation media and pyrolysis temperature for activated carbons development by pyrolysis of potato peels for effective adsorption of endocrine disruptor bisphenol-A, J. Colloid Interface Sci. 466 (2016) 101–112, https://doi.org/10.1016/J.JCIS.2015.12.003.
[37] Q.S. Liu, T. Zheng, P. Wang, J.P. Jiang, N. Li, Adsorption isotherm, kinetic and mechanism studies of some substituted phenols on activated carbon fibers, Chem. Eng. J. 157 (2010) 348–356, https://doi.org/10.1016/J.CEJ.2009.11.013.
[38] I. Bautista-Toledo, M.A. Ferro-García, J. Rivera-Utrilla, C. Moreno-Castilla, F.J.V. Fernández, Bisphenol a removal from water by activated carbon. Effects of carbon characteristics and solution chemistry, Environ. Sci. Technol. 39 (2005) 6246–6250, https://doi.org/10.1021/ES0481169.
[39] J. Xiao, W. Lv, Z. Xie, Y. Tan, Y. Song, Q. Zheng, Environmentally friendly reduced graphene oxide as a broad-spectrum adsorbent for anionic and cationic dyes via $\pi-\pi$ interactions, J. Mater. Chem. A. 4 (2016) 12126–12135, https://doi.org/10.1039/C6TA04119A.
[40] G.K. Ramesha, A.V. Kumara, H.B. Muralidhara, S. Sampath, Graphene and graphene oxide as effective adsorbents toward anionic and cationic dyes, J. Colloid Interface Sci. 361 (2011) 270–277, https://doi.org/10.1016/J.JCIS.2011.05.050.
[41] K. Rathinam, S.P. Singh, Y. Li, R. Kasher, J.M. Tour, C.J. Arnusch, Polyimide derived laser-induced graphene as adsorbent for cationic and anionic dyes, Carbon N. Y. 124 (2017) 515–524, https://doi.org/10.1016/J.CARBON.2017.08.079.
[42] N. Shimodaira, A. Masui, Raman spectroscopic investigations of activated carbon materials, J. Appl. Phys. 92 (2002) 902–909, https://doi.org/10.1063/1.1487434.
[43] Z. Gong, S. Li, J. Ma, X. Zhang, Self-flocculated powdered activated carbon with different oxidation methods and their influence on adsorption behavior, J. Hazard Mater. 304 (2016) 222–232, https://doi.org/10.1016/J.JHAZMAT.2015.10.039.
[44] X. Huang, D. Lv, L. Yan, G. Zhang, Effects of water factors on the effectiveness of EDC adsorption on novel tailored activated carbon, Water, Air, Soil Pollut. 227 (2016) 398, https://doi.org/10.1007/s11270-016-3104-8.
[45] F. Liu, Y. Dai, S. Zhang, J. Li, C. Zhao, Y. Wang, C. Liu, J. Sun, Modification and application of mesoporous carbon adsorbent for removal of endocrine disruptor bisphenol A in aqueous solutions, J. Mater. Sci. 53 (2018) 2337–2350, https://doi.org/10.1007/s10853-017-1705-2.
[46] J.R. Koduru, L.P. Lingamdinne, J. Singh, K.H. Choo, Effective removal of bisphenol A (BPA) from water using a goethite/activated carbon composite, Process Saf. Environ. Protect. 103 (2016) 87–96, https://doi.org/10.1016/J.PSEP.2016.06.038.
[47] Q. Sui, J. Huang, Y. Liu, X. Chang, G. Ji, S. Deng, T. Xie, G. Yu, Rapid removal of bisphenol A on highly ordered mesoporous carbon, J. Environ. Sci. 23 (2011) 177–182, https://doi.org/10.1016/S1001-0742(10)60391-9.